AD-A143 631 CONTROL OF JET FLOWFIELD DYNAMICS(U) MCDONNELL DOUGLAS 1/1
RESEARCH LABS ST LOUIS MO V KIBENS ET AL. 29 FEB 84
MDC-Q1214 AFOSR-TR-84-0551 F49620-83-C-0048

UNCLASSIFIED F/G 20/4 NL

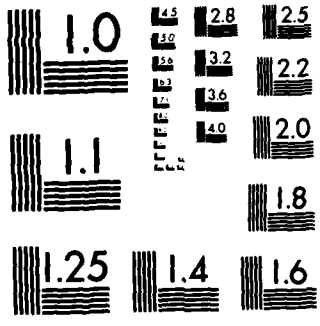

Report MDC Q1214
Contract No. F49620-83-C-0048

CONTROL OF JET FLOWFIELD DYNAMICS

V. Kibens
R. W. Wlezien

McDonnell Douglas Research Laboratories
St. Louis, Missouri 63166

29 February 1984
Scientific Report for the Period 1 January 1983 - 1 January 1984

Approved for public release; distribution unlimited

The views and conclusions contained in this document are those of the authors and should not be interpreted as necessarily representing the official policies or endorsements, either expressed or implied, of the Air Force Office of Scientific Research of the U.S. Government.

Prepared for:

UNITED STATES AIR FORCE
Air Force Office of Scientific Research/AFSC
Bolling Air Force Base, DC 20332

MCDONNELL DOUGLAS RESEARCH LABORATORIES

MCDONNELL DOUGLAS CORPORATION

UNCLASSIFIED

SECURITY CLASSIFICATION OF THIS PAGE

REPORT DOCUMENTATION PAGE

1a. REPORT SECURITY CLASSIFICATION: Unclassified	1b. RESTRICTIVE MARKINGS
2a. SECURITY CLASSIFICATION AUTHORITY	3. DISTRIBUTION/AVAILABILITY OF REPORT: Approved for public release; distribution unlimited
2b. DECLASSIFICATION/DOWNGRADING SCHEDULE	
4. PERFORMING ORGANIZATION REPORT NUMBER(S): MDC Q1214	5. MONITORING ORGANIZATION REPORT NUMBER(S): AFOSR-TR- 84-0951
6a. NAME OF PERFORMING ORGANIZATION: McDonnell Douglas Research Laboratories; 6b. OFFICE SYMBOL (If applicable)	7a. NAME OF MONITORING ORGANIZATION: AFOSR/NA
6c. ADDRESS (City, State and ZIP Code): P.O. Box 516, St. Louis, MO 63166	7b. ADDRESS (City, State and ZIP Code)
8a. NAME OF FUNDING/SPONSORING ORGANIZATION: Department of the Air Force; 8b. OFFICE SYMBOL (If applicable): AFOSR/NA	9. PROCUREMENT INSTRUMENT IDENTIFICATION NUMBER: F49620-83-C-0048
8c. ADDRESS (City, State and ZIP Code): Air Force Office of Scientific Research/AFOSR, Bolling Air Force Base, Washington, DC 20332	10. SOURCE OF FUNDING NOS. — PROGRAM ELEMENT NO.: 61102F; PROJECT NO.: 2307; TASK NO.: A2; WORK UNIT NO.:
11. TITLE (Include Security Classification): CONTROL OF JET FLOWFIELD DYNAMICS (UNCLASSIFIED)	
12. PERSONAL AUTHOR(S): Kibens, Valdis, and Wlezien, Richard W.	
13a. TYPE OF REPORT: Annual Technical; 13b. TIME COVERED: FROM 83 Jan 1 TO 84 Jan 01	14. DATE OF REPORT (Yr., Mo., Day): 1984 February 29; 15. PAGE COUNT: 39
16. SUPPLEMENTARY NOTATION	
17. COSATI CODES — FIELD / GROUP / SUB. GR	18. SUBJECT TERMS (Continue on reverse if necessary and identify by block number): Fluid mechanics; Control of turbulence; Shear layers; Passive control; Jet flows

19. ABSTRACT (Continue on reverse if necessary and identify by block number)

Passive control of shear layer turbulence was investigated experimentally for low subsonic velocity jets from circular nozzles by studying effects of modifying nozzle exit geometry. The indeterminate origin (I.O.) nozzles used, including slanted, stepped and crenelated exit geometries, were so designated because streamwise location of the nozzle lip varies with azimuthal position, unlike standard nozzles, for which the entire termination is at the same streamwise location. Flow visualization and detailed hot-wire measurements were used to observe development and interaction of large-scale turbulent structures in shear layers originating from various sectors of the I.O. nozzles, to determine the influence of instability wave patterns on ensuing flowfield characteristics and to relate observed evolution of three-dimensional large-scale turbulent structures to global properties of the jet flowfield such as velocity profiles and shear layer spreading rates as a function of streamwise distance and azimuthal angle. Results showed pronounced asymmetries in shear layer growth rates, which could be controlled by varying nozzle parameters. The asymmetries

20. DISTRIBUTION/AVAILABILITY OF ABSTRACT: UNCLASSIFIED/UNLIMITED ☒ SAME AS RPT ☐ DTIC USERS ☐	21. ABSTRACT SECURITY CLASSIFICATION: Unclassified
22a. NAME OF RESPONSIBLE INDIVIDUAL: Michael S Francis, Maj, USAF	22b. TELEPHONE NUMBER: 202/767-4935; 22c. OFFICE SYMBOL: AFOSR/NA

DD FORM 1473, 83 APR — EDITION OF 1 JAN 73 IS OBSOLETE

UNCLASSIFIED

SECURITY CLASSIFICATION OF THIS PAGE

18. Subject Terms (continued)

Indeterminate origin nozzles
Asymmetric nozzles
Slanted nozzles
Stepped nozzles
Crenelated nozzles

19. Abstract (continued)

were also confirmed by measurements of azimuthal variation of shear layer turbulent energy as well as mean-velocity profiles. Detailed features of energy transfer from the mean flow into successively larger flow structures were traced by spectral mapping techniques, which display turbulent kinetic energy in physical and wave number space and by mapping energy levels contained in subharmonics of the shear-layer instability frequency at various azimuthal flow sectors.

A-1

PREFACE

The work reported herein was performed by the McDonnell Douglas Research Laboratories in St. Louis, Missouri, for the United States Air Force Office of Scientific Research, Bolling Air Force Base, Washington, DC, under Contract F49620-83-C-0048. The work reported was conducted from 1 January 1983 to 1 January 1984 in the Flight Sciences Department, managed by Dr. R. J. Hakkinen. The principal investigator was Dr. V. Kibens; Dr. R. W. Wlezien was co-investigator. The program technical monitor was Major M. S. Francis.

This technical report has been reviewed and is approved.

R. J. Hakkinen
Director-Research, Flight Sciences
McDonnell Douglas Research Laboratories

D. P. Ames
Staff Vice-President
McDonnell Douglas Research Laboratories

CONTENTS

LIST OF ILLUSTRATIONS

LIST OF ILLUSTRATIONS (continued)

1. INTRODUCTION

This report describes results of the first year of a research program to investigate a series of techniques for passive, active, and interactive turbulence control applied to shear layers of subsonic, axisymmetric jets. The first year of the program dealt with passive turbulence control techniques, which employ variation of nozzle exit shapes and their interactions with inherent flow instabilities as control mechanisms for manipulating jet development.

This research relates to applications for controlling the near-field fluctuating pressure environment and resulting fatigue impact of aircraft powerplants, and reducing the acoustic and infrared signatures of aircraft and missiles and improving the mixing efficiency of ejector nozzles.

Plans for the second year of research are outlined, based on the experience gained from the passive control experiments of the first year's program. The second year will consist primarily of an investigation of active turbulence control through the addition of energy to the flow from external sources using various excitation techniques.

The research described is based on and extends previous MDRL investigations of shear-layer instabilities. It uses techniques developed under previous related IRAD work for describing global dynamics of flowfields. These techniques facilitate handling of large amounts of data through the MDRL PDP 11/70 data acquisition system. To evaluate the effectiveness of various control techniques, the reduced data are displayed in compact formats that demonstrate the effects of three-dimensionality and variations in energy distribution for spatial and wavelength coordinates.

Related MDRL IRAD work is also briefly described.

2. OBJECTIVES

The principal objectives were to observe the development and interaction of shear layers originating from various sectors of indeterminate origin nozzles, to determine the influence of instability wave patterns on the ensuing flowfield characteristics, and to relate the observed three-dimensional, large-scale structure patterns to global properties of the jet flowfield such as entrainment and shear-layer spreading rates as a function of streamwise distance and azimuthal angle.

The specific objectives of the first year's research were:

1. Select a series of indeterminate origin nozzle terminations to evaluate their effectiveness in providing passive control over flowfield development.

2. Perform flow-visualization studies to document global flowfield characteristics.

3. Perform computer-controlled flowfield surveys of selected terminations to demonstrate their effectiveness for turbulence control.

4. Establish the spatial and wave-number distribution of turbulent kinetic energy in the flowfield.

5. Select nozzle shapes for active control tests to be performed during the second year of the program.

3. EXPERIMENTAL APPARATUS

The experiments were performed in the MDRL Flight Sciences Laboratories jet flow facility, which consists of a flow system for generating subsonic air jets from nozzles up to 63.5-mm diameter. Air is supplied by a high-pressure centrifugal blower whose speed is stabilized through feedback control. Flow rates are controlled by computer. The facility includes a three-degree-of-freedom, computer-controlled traverse. The associated data acquisition system uses a PDP 11/70 minicomputer, which also controls experiments.

A typical nozzle installation is shown in Figure 1, along with a specially designed smoke injector which is installed immediately upstream of the nozzle exit. The injector introduces either smoke or helium into the boundary layer ahead of the nozzle exit through a thin, circumferential slit in the injector wall. The smoke is fed from a central distribution point through four separate tubes into the injection chamber and is then forced into the boundary layer through the downstream-facing injection slit. This procedure for introducing smoke provides more effective visualization of shear-layer features than techniques that introduce smoke into the entire flowfield.

Figure 1. Passive-control nozzle installation.

3.1 Nozzle Geometry

Nozzles were available from a concurrent MDRL IRAD project dedicated to supersonic jets. Either slanted, stepped, or crenelated, they are classified as indeterminate-origin (I.O.) nozzles. The designation was chosen to distinguish them from nozzles for which the lip is at the same streamwise location. The dominant shear-layer instability-wave patterns tend to be axisymmetric for standard circular nozzles. By initiating the flow from indeterminate-origin nozzles, the axial symmetry is broken; and new, three-dimensional instability wave patterns may develop.

The slanted and stepped nozzles are designated by the letters C-H, as shown in Figure 2, depending on the length of the extension with respect to the nominal nozzle origin, which is indicated by the dashed lines in Figure 2. Prefixes 1 and 2 designate nozzle diameters of 25.4 and 63.5 mm, respectively. For example, a 25.4-mm slanted nozzle with an extension of D/4 is designated nozzle 1C. Figure 2b shows photographs of series 1 nozzles.

The full set of I.O. nozzles includes crenelated nozzles, which conceptually are extensions of the stepped nozzles with two or more tabs arranged evenly around the nozzle perimeter. The upstream section of all nozzles is an axisymmetric, constant-diameter pipe. The length of the nozzle from the end of the contraction to the jet origin is constant, equal to 63.5 mm for Series 1 and 158.8 mm for Series 2 nozzles to ensure approximately the

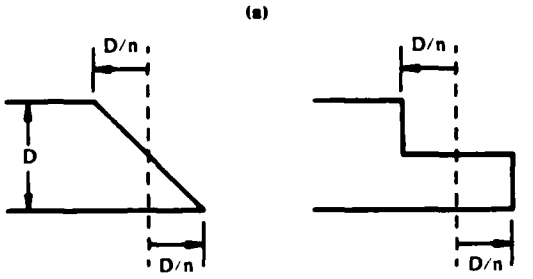

Slanted nozzle

n	Designation
4	C
2	D
1	E

Stepped nozzle

n	Designation
4	F
2	G
1	H

Nozzle sizes: Series 1: D = 25.4 mm
Series 2: D = 63.5 mm

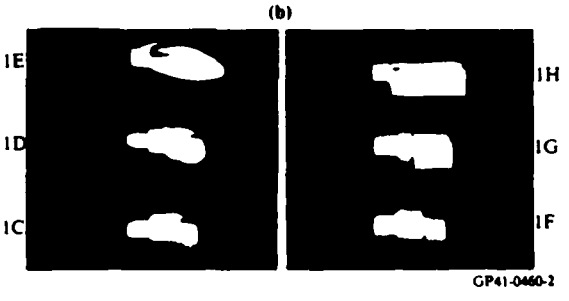

Figure 2. (a) Nomenclature for indeterminate-origin (I.O.) nozzles and (b) photographs of the Series 1 nozzles.

same boundary-layer thickness for nozzles in a particular series. The distance from the contraction to the nearest upstream position varies, depending on the nozzle designation.

4. TEST RESULTS

4.1 Flow Visualization

Flow visualization was used to classify the flow corresponding to the various nozzle geometries and exit velocities according to their potential for passive turbulence control, and to select a manageable set of the most promising configurations for more detailed investigation.

The standard circular nozzle was used as a reference configuration, and deviations observed in I.O. nozzle flows were noted. Flows from circular nozzles have been extensively studied; results have demonstrated that mixing can be controlled by modification of large-scale structures. Some work also has been done on nonaxisymmetric terminations, such as rectangular and elliptic nozzles (References 1 and 2). It has been demonstrated that the geometry of the nozzle exit and the interactions of large-scale structures play important roles in the mixing characteristics of the ensuing jet. Since the origin of each shear-layer sector for circular, rectangular, or elliptic nozzles is at the same streamwise location, there is phase synchronization for the instability-wave system. The I.O. nozzles are distinguished by the feature that for a given streamwise position in the jet, the distance from the nozzle lip varies with the azimuthal position; and therefore, there is an azimuthal variation in the amplitudes of the instability waves. As a first-order approximation, we may expect wave amplitudes to be proportional to the "age" of the particular shear-layer sector at a given streamwise location.

Figures 3-6 illustrate the qualitative changes in instability-wave development for I.O. nozzles, compared to the standard circular nozzle. In all four cases, the nozzle section upstream of the termination is circular and has a diameter of 25.4 mm; the velocity is 4 m/s. The symmetry of the circular nozzle flowfield is evident in Figure 3. Symmetry extends beyond the end of the potential core region, and mean properties of the entire flow can be determined by examining one azimuthal plane and assuming axial symmetry. Departure from symmetry for a slanted nozzle termination is evident in Figure 4, which shows the flowfield for nozzle 1C. This flow satisfies the intuitive expectation that wave crests of the instability-wave system should be aligned with the nozzle exit and that the amplitude of the instability waves should be proportional to the distance from the nozzle lip. Figure 5 shows flowfield

GP41-0460-3

Figure 3. Jet flowfield characteristics: axisymmetric nozzle; diameter D = 25.4 mm and velocity U = 4 m/s.

GP41-0460-4

Figure 4. Jet flowfield characteristics: slanted nozzle 1C; U = 4 m/s.

GP41-0460-5

Figure 5. Jet flowfield characteristics; slanted nozzle 1E; U = 4 m/s.

GP41-0460-6

Figure 6. Jet flowfield characteristics; stepped nozzle 1G; U = 4 m/s.

characteristics of nozzle 1E. The instability wave system has reached the nonlinear vortex rollup stage for the upper sector of the shear layer before it has left the last part of the nozzle termination. Inclination of the vortices is approximately perpendicular to the flow direction, as opposed to the vortex system shown in Figure 4.

Figure 6 shows the flow from the stepped nozzle 1G at 4 m/s. Development of the instability waves in this flow goes counter to the expectation that the two displaced sectors of the nozzle will each initiate its own instabilty-wave system.

The flows shown in Figures 3-6 illustrate two general classes of shear-layer behavior: (1) externally originating shear-layer instabilities for which the development of the instability waves takes place downstream of the nozzle exit (Figures 3 and 4) and for which the nozzle lip-line geometry determines the phase relationship of the initial wave fronts; and (2) the class of internally originating instabilities (Figures 5 and 6) in which the characteristics of the wave system are determined primarily by one sector of the shear layer, namely, that leaving the nozzle at the farthest upstream position. For the second class of flows, the main features of the instability wave system are established before the end of the nozzle, and the role of the lip line is more complex than for externally originating shear-layer instabilities.

Several variations of the two main classes of shear-layer development were observed as functions of jet velocity, nozzle diameter, and initial shear-layer thickness. In Figure 7, the visualization of the flow from nozzle 1C at a velocity U = 20 m/s shows that the spacing between successive vortices

Figure 7. Jet flowfield characteristics; slanted nozzle 1C; U = 20 m/s.

in the instability wave train has decreased and that the point of vortex rollup has moved closer to the nozzle exit than is the case for the flow from the same nozzle at a lower speed (Figure 4). The wave system, however, is clearly originating externally.

Figure 8 shows the flowfield of nozzle 2C at a velocity of 30 m/s. The initial momentum thickness of this flow is less than that for nozzle 1C. The vortex-system phase lines are clearly parallel to the nozzle exit, and the flow belongs to the class of externally originating shear layer instability systems.

Figure 9 shows the flowfield for nozzle 2E at 30 m/s, the same velocity as that for Figure 8. This instability-wave system, however, originates internally. Comparing Figures 9 and 5, we see that while only two discrete vortices appear within the confines of the nozzle termination geometry envelope for nozzle 1E at 4 m/s, a series of constant-phase fronts perpendicular to the flow direction forms sequentially along the slanting lip line for nozzle 2E at 30 m/s. The strength of the wave fronts decreases with the vertical distance above the lip line. The photograph suggests that the shear-layer sector originating at the azimuthal position $\phi = 180^{o}$ plays a key

GP41-0460-8

Figure 8. Jet flowfield characteristics, externally generated instability wave system; slanted nozzle 2C; U = 30 m/s.

GP41-0460-9

Figure 9. Jet flowfield characteristics; internally generated instability wave system; slanted nozzle 2E; U = 30 m/s.

role in determining the instability wave pattern, where $\phi = 0^{o}$ is defined as the angular position of the center point of farthest streamwise sector of the nozzle lip. The lineup of successive vortices along the lip line suggests that lateral communication of the instability-wave phase pattern to the nozzle lip may be the key to establishing the regular series of wave fronts along the slanting lip line. This instability-wave pattern clearly is complex, three-dimensional, and qualitatively distinct from that of the externally developing shear-layer instability systems.

The flowfield of the step nozzle 2G in Figure 10 exhibits two independently developing shear layers that originate at the separate step faces. In Figure 11, which illustrates flow from the stepped nozzle 2F, the upper and lower shear layers appear to undergo independent, but similar instability-wave development. The vortex lines orginating in the two instability-wave patterns appear to join in the middle of the photograph.

Figure 12 shows two views of the flow from a crenelated nozzle. This flow is similar to a stepped-nozzle flow in that the shear layers originating in the upstream sectors of the nozzle develop earlier than those originating at the ends of the tabs. In the top view, the wave systems are in phase for the upper and lower shear layers even though they are separated by intervening tabs, indicating communication of phase information across the body of the flow or through the side boundary layers of the tabs.

GP41-0460-10

Figure 10. Jet flowfield characteristics; stepped nozzle 2G; U = 20 m/s.

GP41-0460-11

Figure 11. Jet flowfield characteristics; stepped nozzle 2F; U = 30 m/s.

In Figure 13, for a four-tab crenelated nozzle, similar phase coherence is evident among the structures developing between the tabs.

The flow-visualization tests demonstrate that passive control of the jet flowfield is possible by varying the nozzle exit termination shapes and that

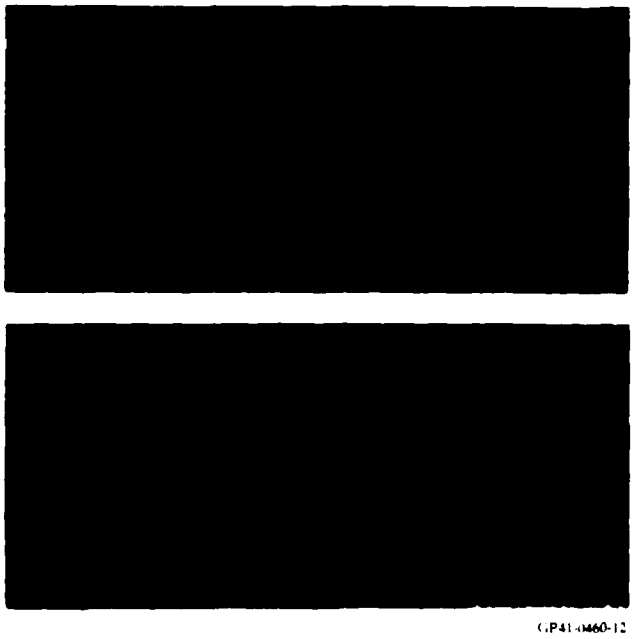

Figure 12. Jet flowfield characteristics; two-tab crenelated nozzle; tab extension = D/2; D = 63.5 mm; U = 30 m/s.

Figure 13. Jet flowfield characteristics; four-tab crenelated nozzle; tab extension = D/2; D = 63.5 mm; U = 30 m/s.

interaction of the three-dimensional instability-wave structures is the key to controlling development of jets. By using either the broken lip line of the step or crenelated nozzle or the continuous lip line of the slanted nozzle, and setting a specific velocity and boundary-layer thickness, it is possible to select a variety of initial conditions that modify characteristics of the coherent motion determined by the initial shear-layer instability.

4.2 Streamwise Scale Development

Whereas flow visualization allowed broad categorization of a large number of possible flows, hot-wire measurements were used to evaluate the effectiveness of passive control in each. Mean and unsteady velocity fields were examined for evidence of the degree to which the large-scale structures developing from the instability-wave systems persist into the main body of the jet flowfield and distort it from the reference of a comparable circular jet. Nozzles 1C and 1G were selected as most effective in modifying the gross jet flowfield through passive control on the basis of shear-layer spreading rate measurements. In the following sections, the flows from these nozzles are described in detail.

The general approach employed in examining flows from the various nozzles was to (1) measure gross properties such as mean velocity fields and momentum thickness distribution in the streamwise and azimuthal directions; (2) determine the overall distortion of the jet compared to the reference jet; and (3) document through spectral mapping the flow of energy from the mean flow into the turbulent motion of the shear-layer, starting with the instability-wave system in the early shear layer. This approach describes mechanisms through which the nozzle shape influences the developing instability-wave system and produces three-dimensional turbulent scale interactions, which constitute passive flowfield control.

Figure 14 shows the streamwise development of the distribution of turbulent kinetic energy among Strouhal numbers for an axisymmetric nozzle. The data were taken along the line on which the mean velocity equals 95% of the jet exit velocity U_o. Coordinates for this line were determined by an appropriate algorithm operating on data obtained from a hot-wire probe traversed under computer control. For the 25.4-mm-diam axisymmetric nozzle (Figure 14), energy concentrations are seen at St = 3.3, 1.6, and 0.8. Spectral mapping is shown applied to slanted nozzle 1D in Figure 15 and to a

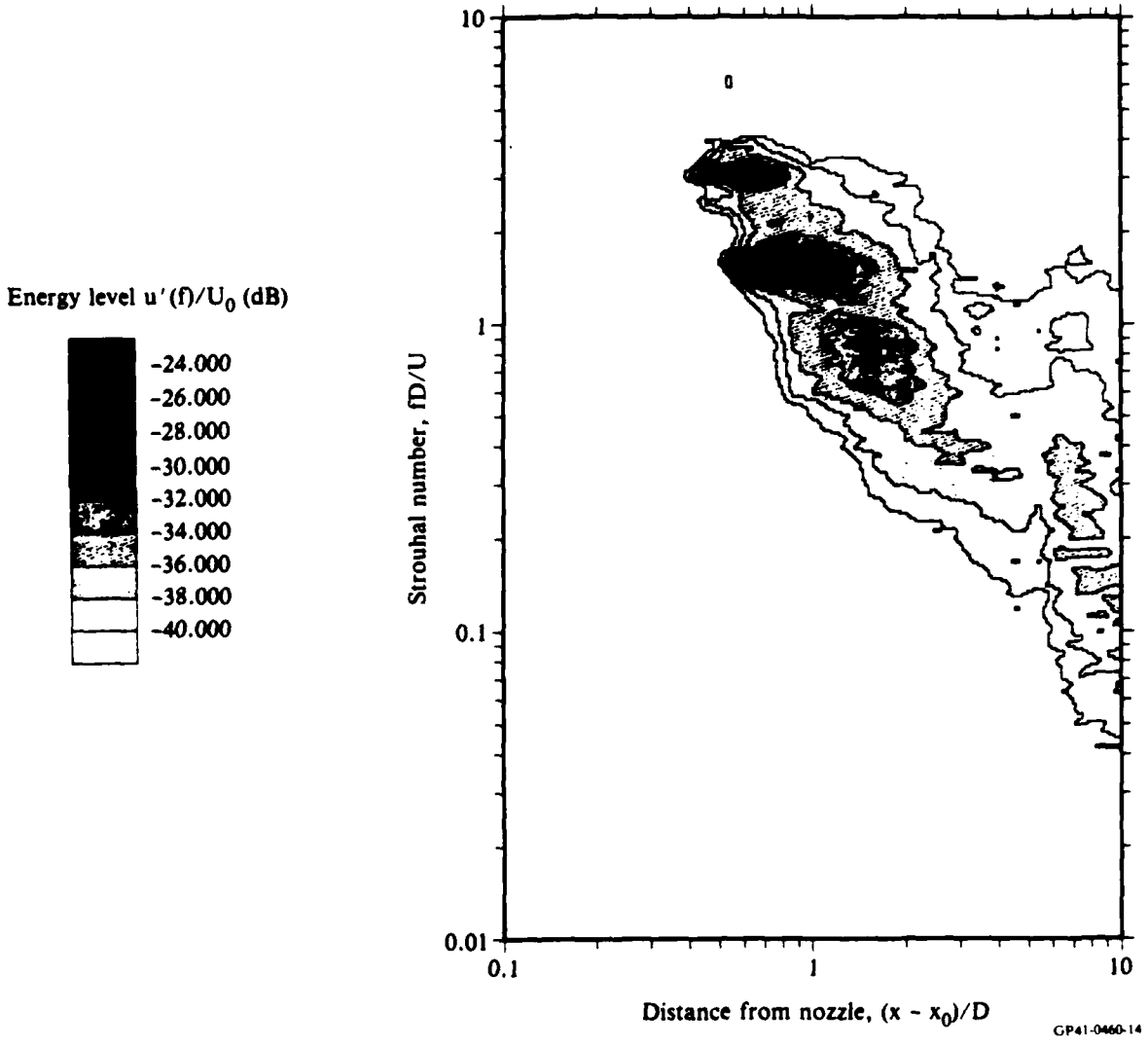

Figure 14. Streamwise spectral development, axisymmetric nozzle; D = 25.4 mm; U = 30 m/s; $y = y|_{0.95\,U_0}$.

63.5-mm-diameter axisymmetric nozzle in Figure 16. Similar plots were generated for all nozzles tested.

Spectral maps for each nozzle geometry and flow velocity were processed to yield a single average frequency associated with a particular streamwise location $(x - x_0)/D$. This frequency value was generated by first obtaining a spectrum at a particular value of $(x - x_0)/D$ and then calculating the average of the energy-weighted frequencies, where the limits of integration were taken

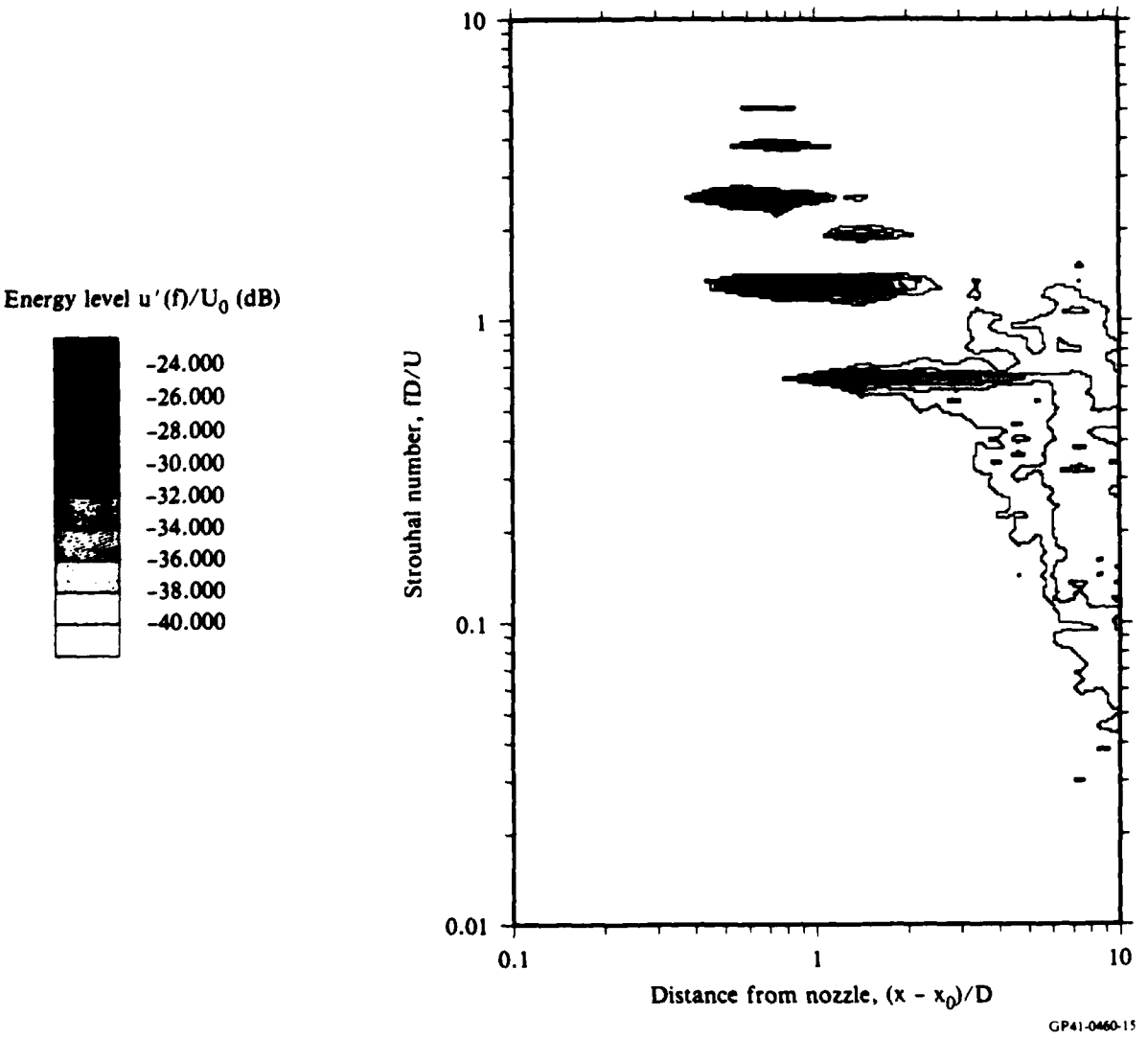

Figure 15. Streamwise spectral development, slanted jet 1D; U = 31.5 m/s; Azimuthal angle $\psi = 0°$; $y = y|_{0.95\ U_0}$.

to be the frequencies at which the energy level dropped below the -40dB level. This procedure is well defined for each flow and assigns a dominant frequency to each streamwise location without subjective judgement. The mean Strouhal number as a function of streamwise distance is plotted in Figure 17 for a variety of nozzle configurations and azimuthal positions. The data for all configurations tested, including those not shown on the plot, appear to exhibit universal behavior. The curve remains virtually unchanged if replotted as a Strouhal number formed with the local half-velocity radius since the half-velocity location as a function of streamwise distance lies

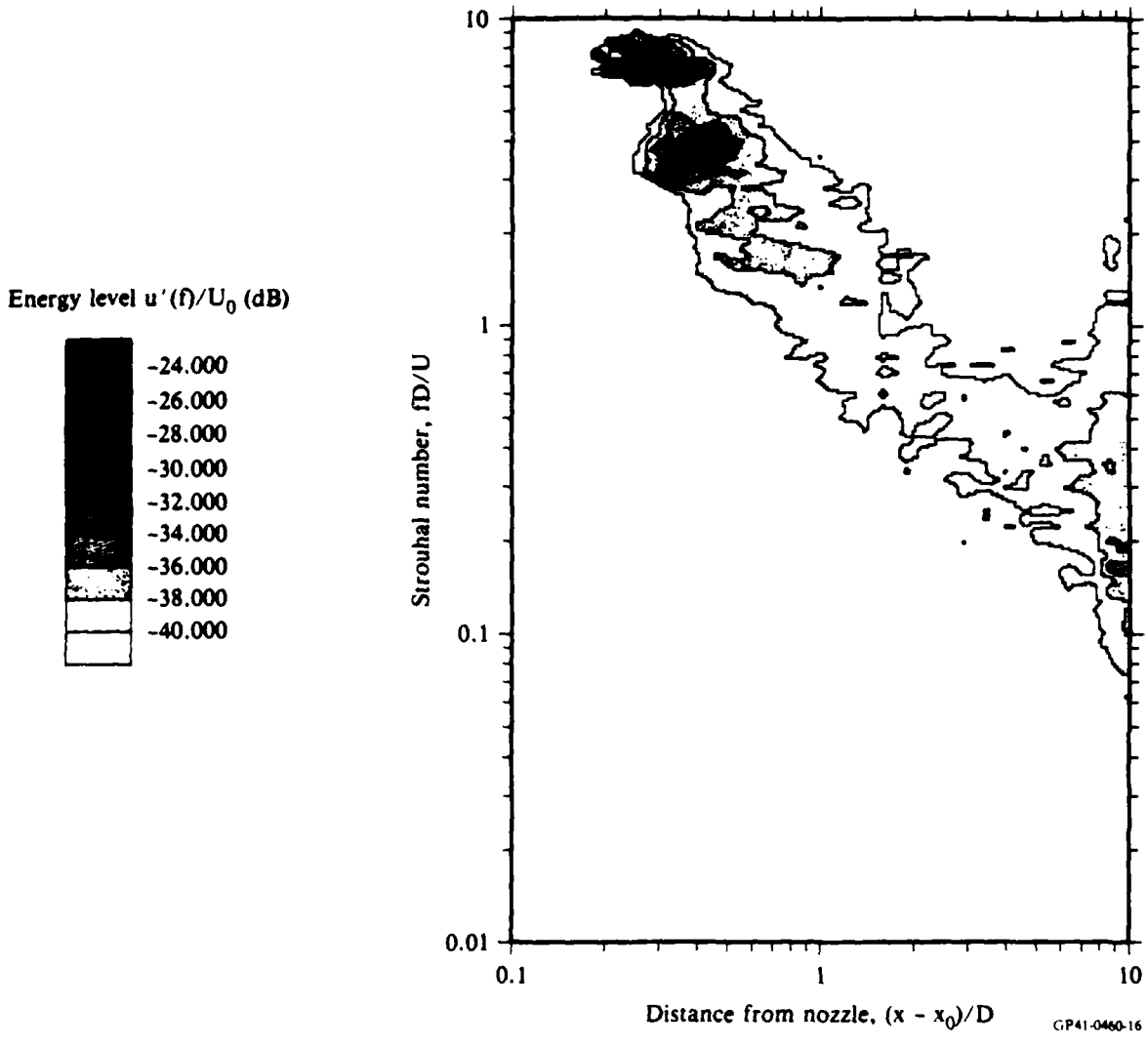

Figure 16. Streamwise spectral development, axisymmetric nozzle; D = 63.5 mm; U = 40 m/s; $y = y|_{0.95\,U_0}$.

approximately on the nozzle lip line. Replotted in terms of Strouhal number based on the local momentum thickness, the data appear as in Figure 18. If we take the Strouhal number to represent the ratio of the reference length scale, either D or θ, to the wavelength of the dominant oscillation at a given streamwise location, then we conclude from Figure 17, that turbulent scales increase with streamwise distance by approximately a factor of 10 with respect to D over a distance $x-x_o \cong 10D$ and from Figure 18, that they decrease by approximately a factor of 5 over the same streamwise distance when compared to

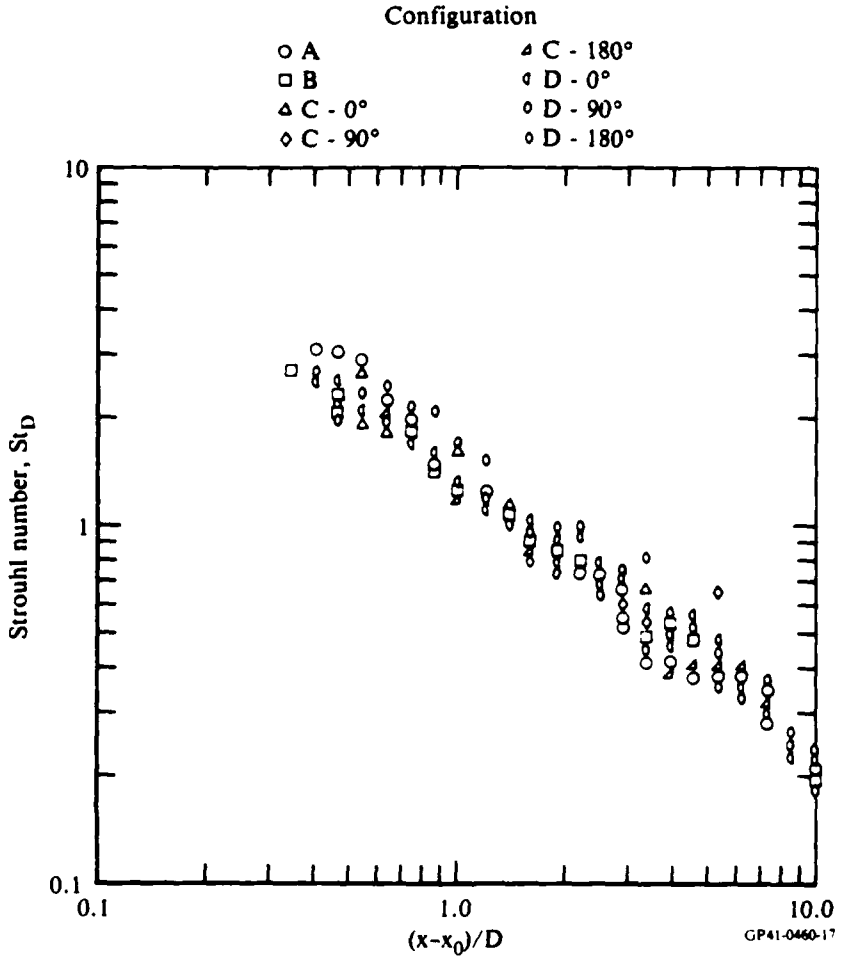

Figure 17. Mean St_D variation with distance from nozzle lip along the 0.95U line.

the local momentum thickness. The universal curve applies for the range of velocities tested, from 20 to 60 m/s. For a wide range of nozzle exit shapes and velocities, the development of a shear layer, starting from the line of separation from the nozzle exit, is constrained to follow an identical path in terms of permissible instability wavelengths and turbulent eddy sizes developed at a given streamwise distance from the separation point. The data were remarkable in the consistency with which they adhered to the universal curve of Figure 17.

We conclude that passive control of jet shear layers is therefore limited to changing the total amount of kinetic energy residing in the coherent motion whose scale is specified for a particular streamwise location. The

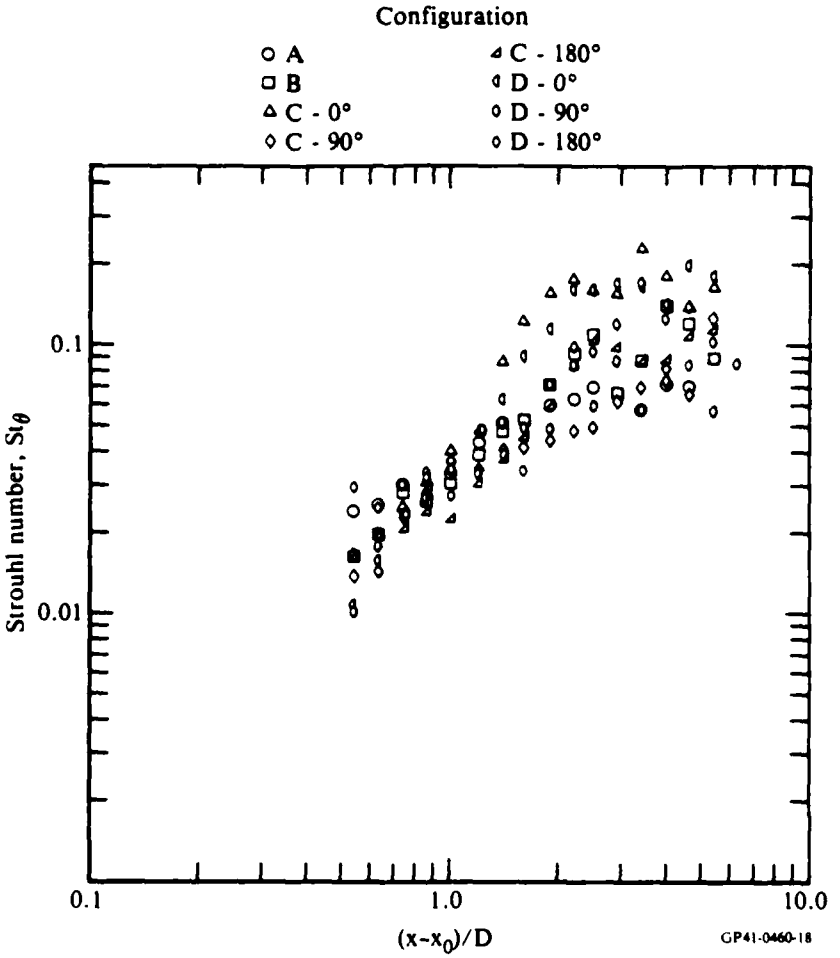

Figure 18. Mean St_θ variation with distance from nozzle lip along the 0.95U line.

limitations imposed by this constraint still leave much variety in the possible spatial arrangements of energy concentrations. Although the constraint imposes a fixed range of eddy sizes for a given distance from the lip, it is possible to obtain a wide variety of three-dimensional initial conditions from which to select potential passive control configurations by varying the streamwise location of the separation point with the azimuthal position.

4.3 Mean Velocity and Momentum Thickness

One of the early conclusions to emerge from tests comparing momentum thickness development is that Series 1 nozzles are more effective than Series 2 nozzles as passive control devices for circular jets. One reason for the

difference is that the initial value of R/θ is ~ 90 for Series 1 nozzles at the nominal test velocity of 30 m/s, whereas for Series 2 nozzles this ratio is approximately 120. According to previous MDRL work (Reference 3), coupling between the initial shear-layer instability waves and the so-called preferred jet-mode or jet-column instability ceases for momentum thickness values in the range 100 < R/θ 120. For R/θ < 100, initial shear-layer instability waves develop into a system of vortices whose interaction is the cause of shear-layer scale enlargement persisting to the end of the potential core. For R/θ > 120, formation of the vortex system from the initial instability waves takes place, just as in the previous case, but the energy in the coherent-wave system does not penetrate to the end of the potential core. Instead, a new wavelength selection process is initiated that is independent of the initial instability frequencies and generates the preferred jet-mode frequency. Since passive control consists of manipulating the geometry of the initial wave system, it is to be expected that the technique will be most effective for thick initial boundary layers, for which R/θ is < 100. Representative hot-wire test results obtained from Series 1 nozzles are described below.

Figure 19 compares the mean velocity fields taken in the cross-sectional plane of the jet at x/D = 4 for inclined nozzle 1C and stepped nozzle 1G. The

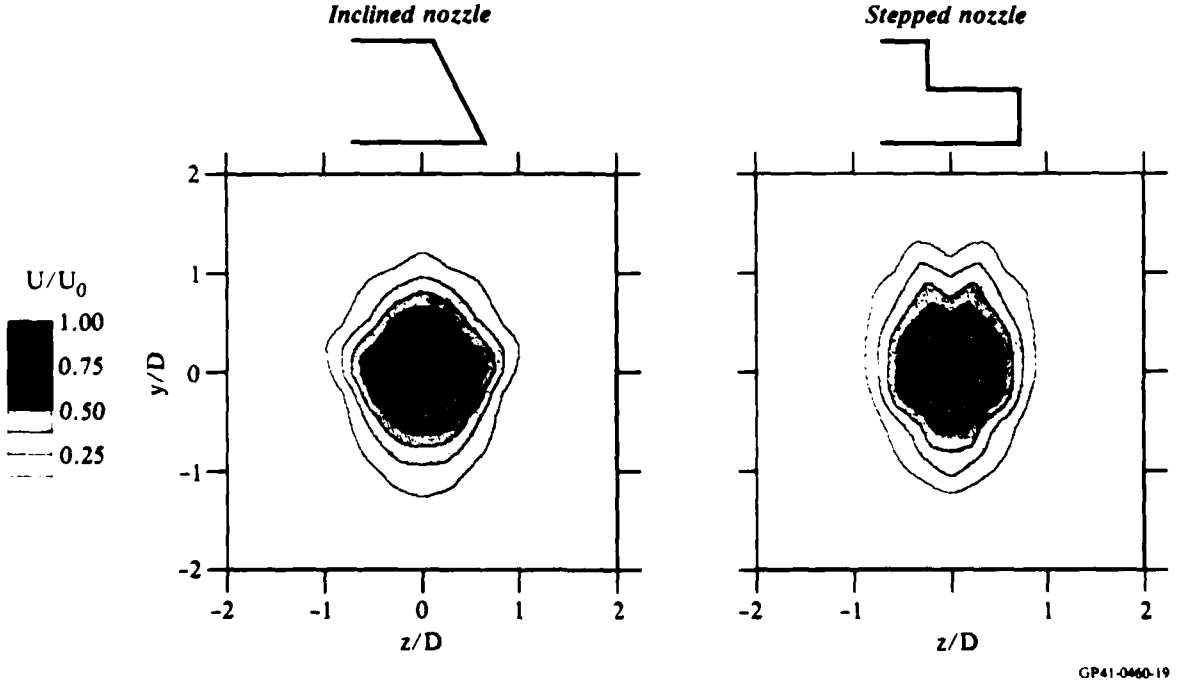

Figure 19. Mean velocity contours for nozzles 1C and 1G; x/D = 4; U_0 = 30 m/s.

equal-velocity contours for both nozzles exhibit a consistent asymmetry, as opposed to the reference jet for which the contours are circular. Both jets are elongated along the z-axis, or along the radial lines $\psi = 0^o$ and 180^o ($\psi = 0^o$ corresponds to the negative z-axis and $\psi = 180^o$ to the positive z-axis).

In Figure 20, the momentum thickness of the shear layers at the azimuthal locations $\psi = 0^o$, 90^o, and 180^o is plotted as a function of streamwise distance and compared to the corresponding momentum thickness for the reference nozzle. For both nozzles, the shear-layer momentum thickness grows faster than that of the reference nozzle for $\psi = 0^o$ and 180^o, and more slowly for $\psi = 90^o$. Data are presented as a function of distance from the nominal nozzle origin. For $x/D < 1.5$, the data for $\psi = 0^o$ lie below the reference curve because of the short development distance for the lower shear layer. For $x/D > 2$ the upper and lower shear layer sectors have increased in thickness above that of the reference case. The maximum momentum thickness attained by the step nozzle at $x/D = 4$ is as much as twice that for the reference case. Figure 21 shows a radial plot of the momentum thickness for nozzle 1C at $x/D = 4$, where $\psi = 0^o$ and 180^o exhibit the maximum values of θ/D. The minimum growth is along the lines $\theta = 60^o$ and 300^o.

In Figure 22 a component of the turbulent energy, defined as $\frac{8}{D^2U_o^2}\int_o^\infty u^2 r\, dr$, is plotted as a function of x/D for nozzles 1C and 1G. For both cases, energy is lower in the shear-layer sector centered on $\psi = 0^o$ than that for $\psi = 180^o$ up to a crossover point at approximately $x/D = 2$. The levels are then reversed, and turbulent activity is higher in the shear-layer sector that originates farthest downstream.

It is possible to generate heuristic arguments explaining this effect in terms of a cross-stream influence from the upper to the lower shear layer. The validation of such modeling, however, requires more detailed experimental data on the degree of mutual influence of the upper and lower shear layers. We are justified in concluding that since the approach flow to the nozzle termination is axisymmetric, the explanation for the asymmetry in growth must lie in (1) the azimuthal variation of the initial instability-wave systems and that of the large-scale structures developed from them, and (2) the resulting three-dimensionality of their consequent interactions. Another heuristic argument for explaining the greater rates of growth of the upper and lower shear layers of nozzle 1C, compared to those of the side shear layers, derives

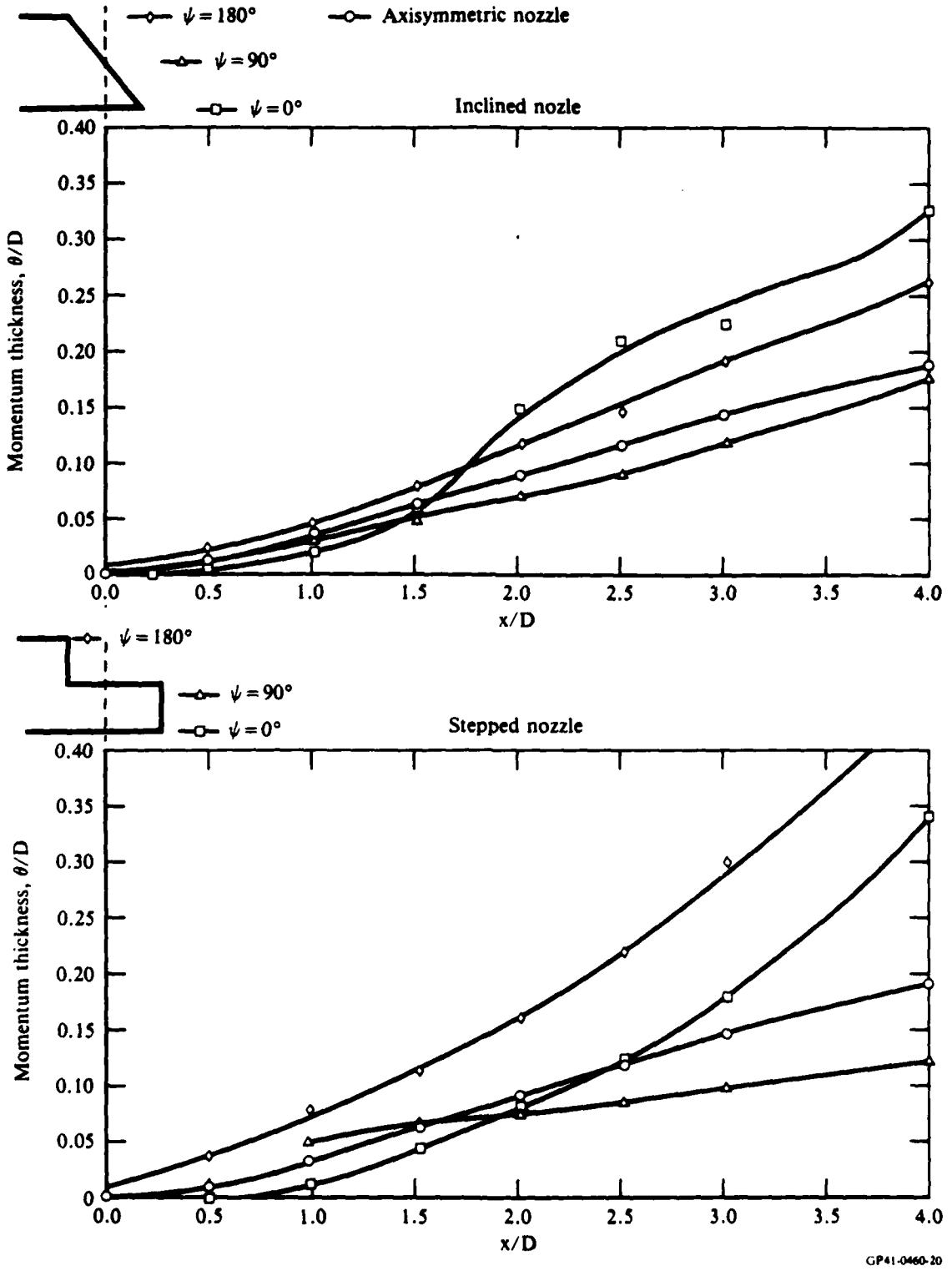

Figure 20. Azimuthal variation of shear-layer momentum thickness for nozzles 1C and 1G; U_0 = 30 m/s.

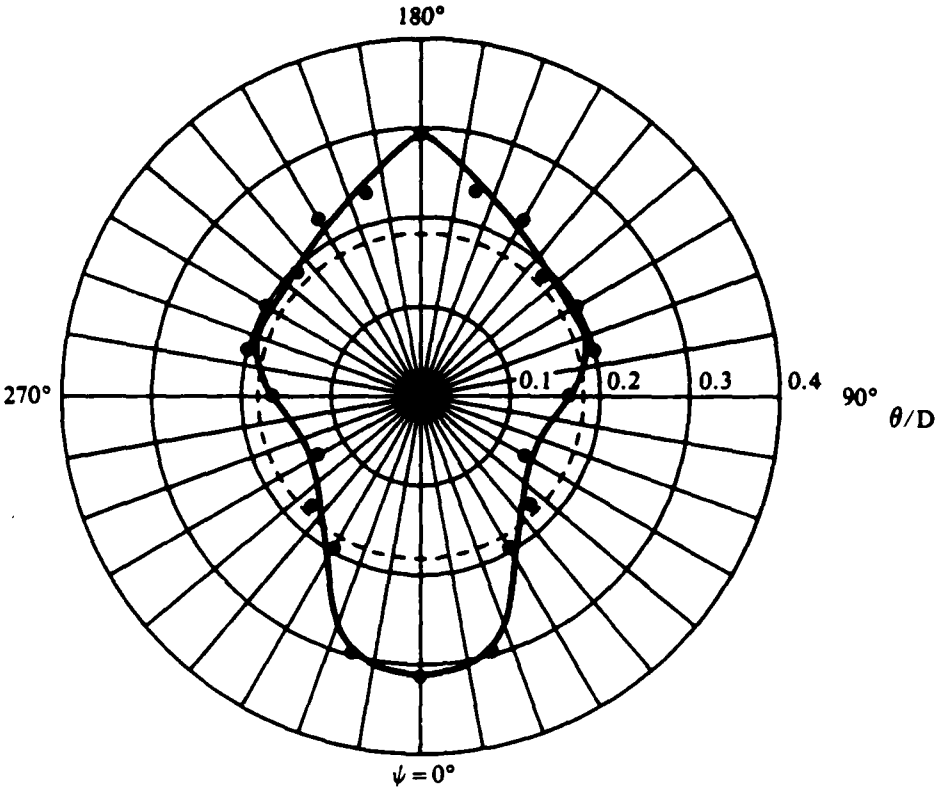

Figure 21. Azimuthal variation of momentum thickness; nozzle 1C; x/D = 4; U_0 = 30 m/s.

from the fact that the inclined vortex system that grows from the initial instability waves contains zero streamwise vorticity at $\psi = 0^{\circ}$ and 180°, and a maximum streamwise vorticity component at $\psi = 90^{\circ}$ and 270°. Since generation of streamwise vorticity plays a role in the breakdown of discrete vortices, the side sectors of the jet may be inherently more sensitive to vortex perturbations and may not be able to employ the interaction of successive vortices for momentum thickness growth.

4.4 Lateral Spectral Development

Figures 23-28 demonstrate techniques that are sufficiently sensitive to describe the variation of turbulent energy in spatial and frequency coordinates, and that can be used as tools to evaluate changes in the flowfield resulting from modifications of nozzle termination geometry. The techniques comprise a high-resolution intermediate evaluation of the flowfield dynamics that is unavailable if only the global results such as noise or entrainment are measured.

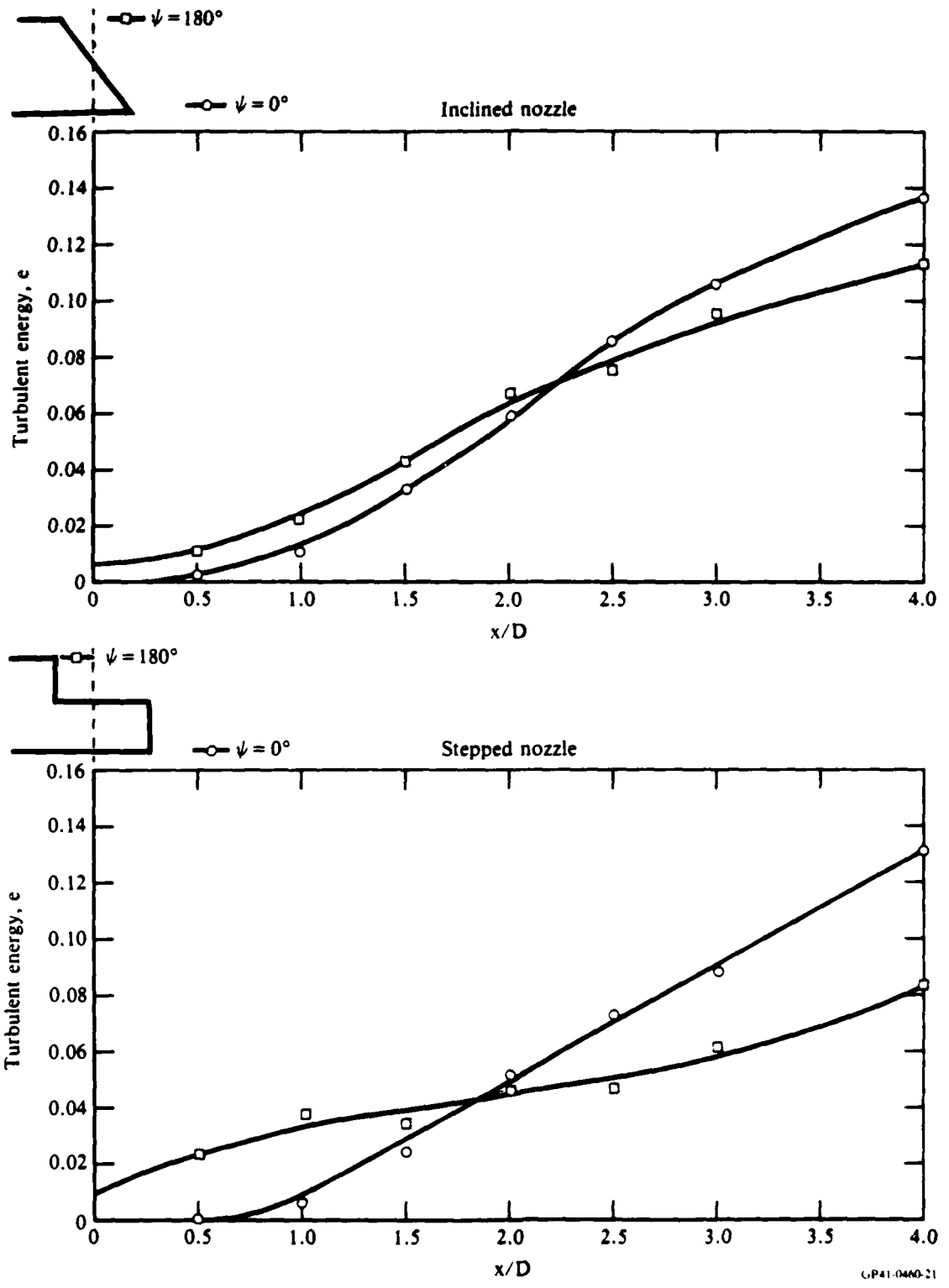

Figure 22. Azimuthal variation of shear-layer streamwise turbulent energy component for nozzles 1C and 1G; $U_0 = 30$ m/s.

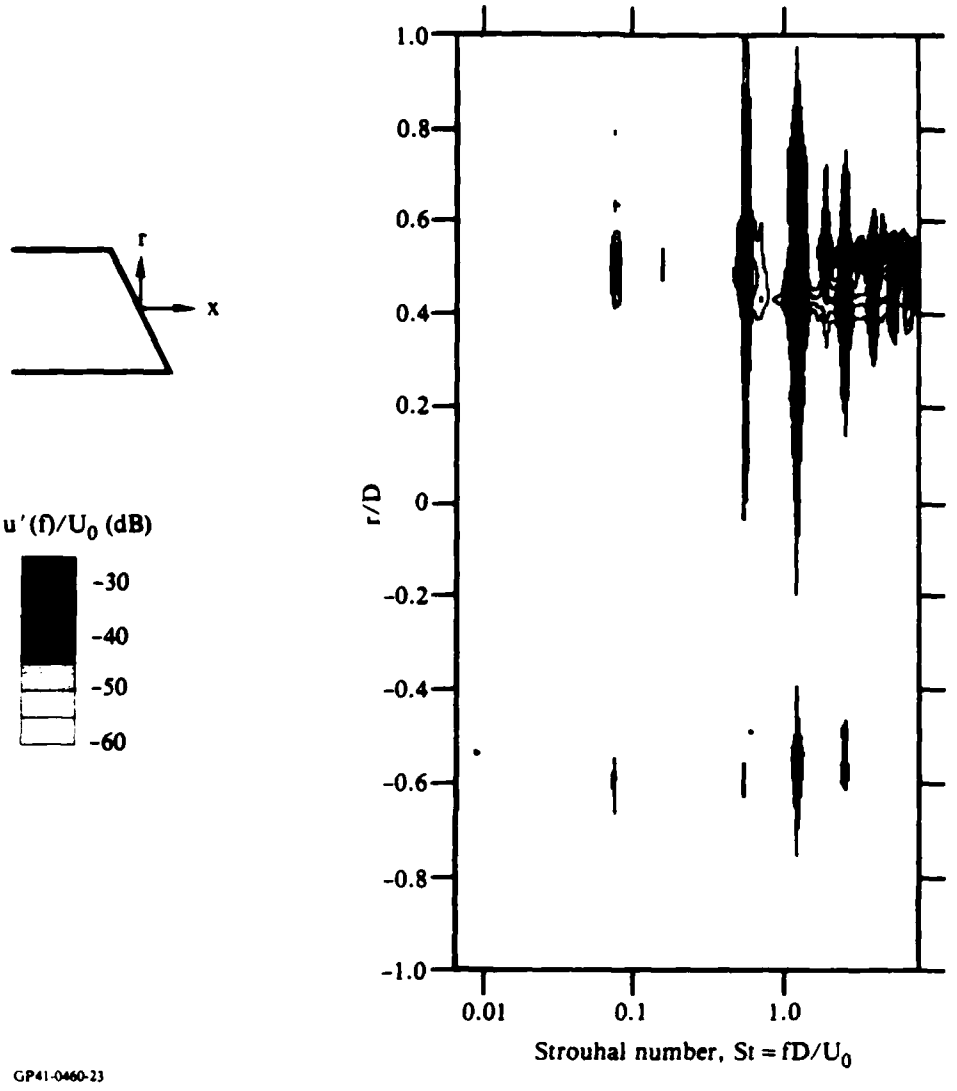

Figure 23. Spectral map for nozzle 1C; x/D = 0.5; U_0 30 m/s.

Figures 23-25 show the lateral distribution of the streamwise component of turbulent energy at three streamwise locations in the form of spectral maps derived from a series of 25 velocity spectra taken along the radial lines ψ = 0^o and 180^o for nozzle 1C. Unsteady flowfield data arranged in spectral maps offer a means of following energy transfer from small to large scales in the developing shear layer while permitting a spatial survey of energy throughout the flowfield. Figure 23 shows characteristics of the early shear layer at x/D = 0.50. This location represents the distance from origin $(x-x_o)/D$ = 0.75 for the upper shear layer (ψ = 180^o) and $(x-x_o)/D$ = 0.25 for the lower shear

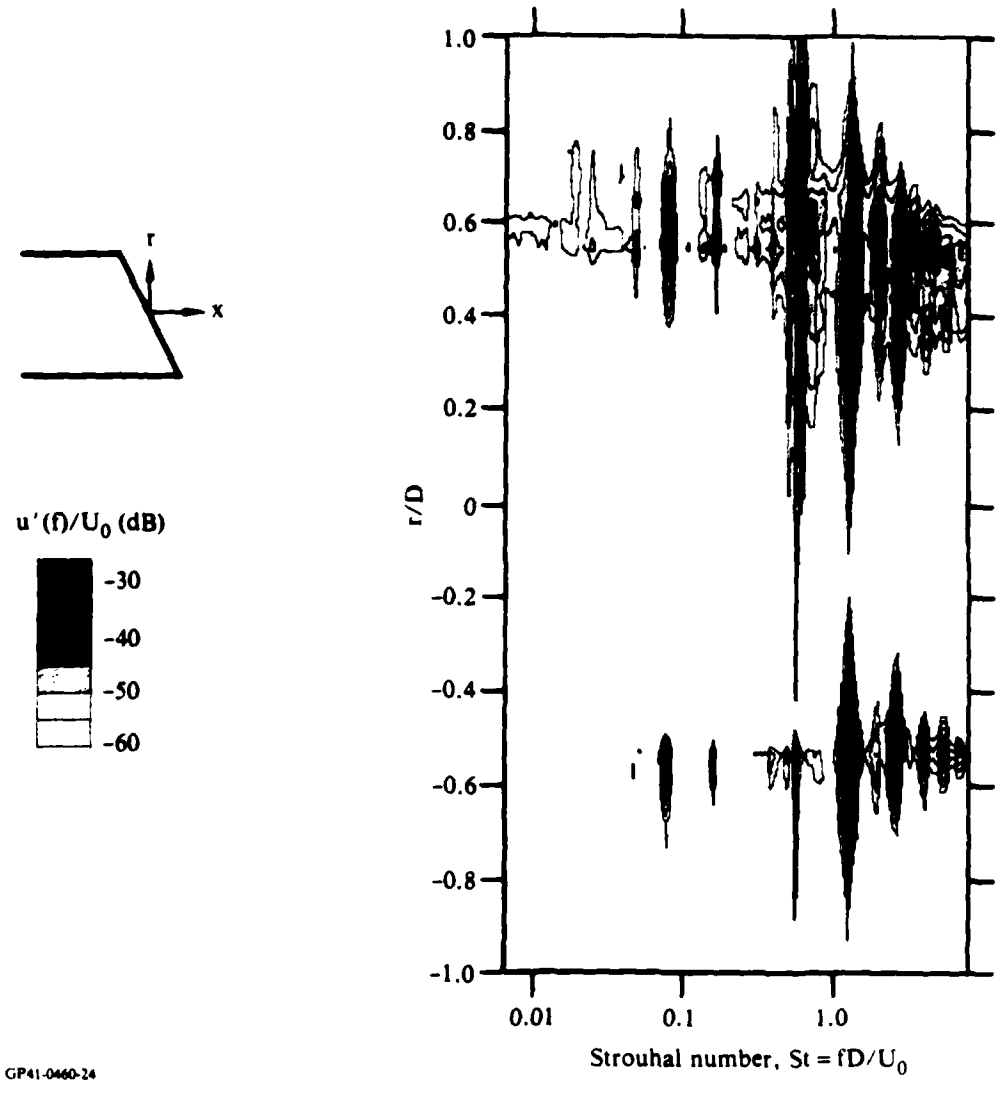

Figure 24. Spectral map for nozzle 1C; x/D = 0.75; U_0 30 m/s.

layer ($\psi = 0^o$). Figure 23 accordingly displays a higher energy concentration in the upper shear layer (r/D = 0.5) than the lower shear layer (r/D = -0.5). The energy is concentrated in discrete bands representing the process of development of the shear-layer instability wave. The upper shear layer exhibits peaks at Strouhal numbers of 2.8, 1.4, and 0.65. The highest energy level is in the peak at St = 1.4. The lower shear layer, whose development has spanned only a streamwise distance $(x-x_o)/D = 0.25$ also shows maximum energy in the frequency band corresponding to St = 1.4, suggesting that it does not develop independently but is influenced by the wave-front structure of the more highly developed upper shear layer.

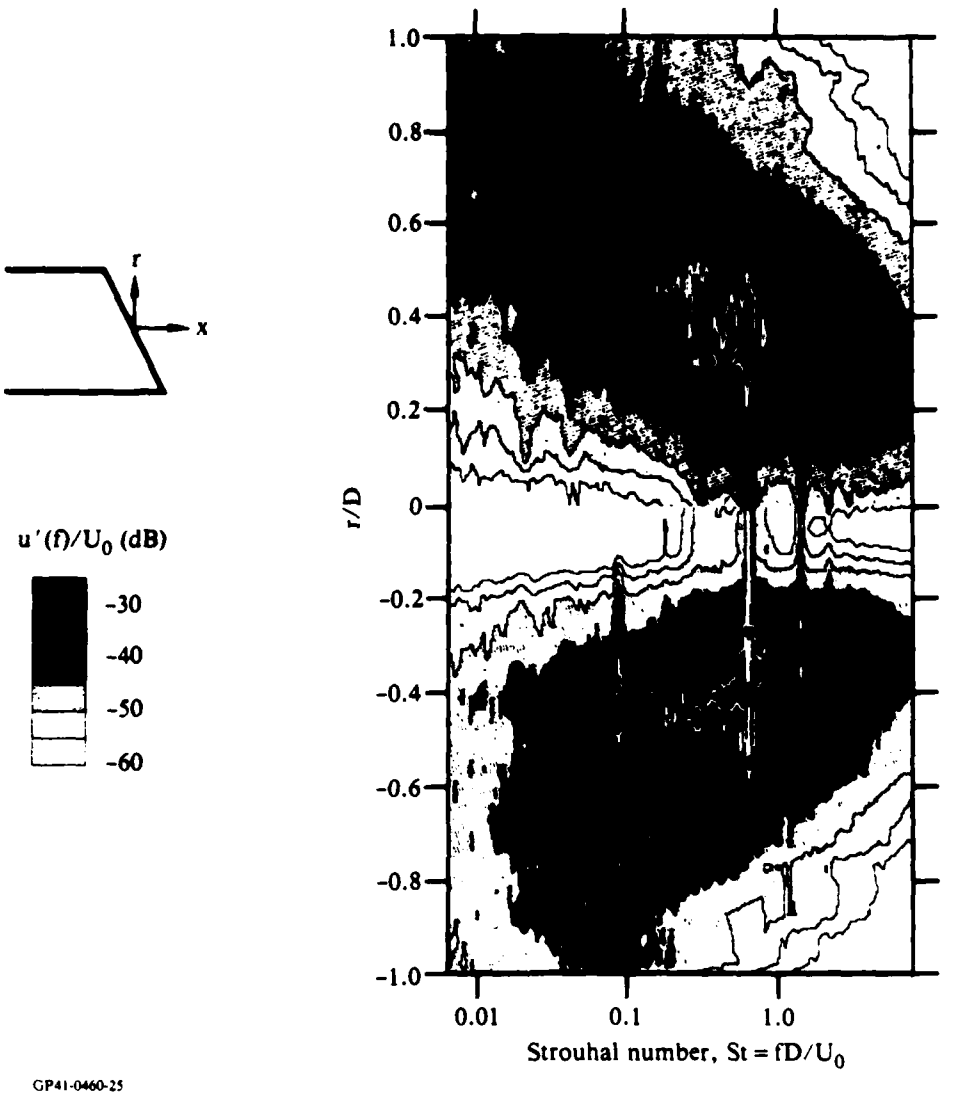

Figure 25. Spectral map for nozzle 1C; x/D = 3; U_0 = 30 m/s.

In Figure 24, for the streamwise location x/D = 0.75, the matching of the spectral signatures of the upper and lower shear layers is even more evident. The peak at St = 1.4 is dominant, and its influence in the upper shear layer reaches across the centerline of the jet to r/D = -0.2; it also has the broadest region of influence in the lower shear layer. The subharmonic at St = 0.65, however, is very strong in the upper shear layer, although it is barely visible in the lower one. At x/D = 0.75 (Figure 24) the upper shear layer is distincly more energetic than the lower one.

At x/D = 3.0 (Figure 25) the roles of the two shear layers are reversed, as suggested in Figures 20 and 22, and the lower shear layer has become the more energetic of the two. The spectrum peak at St = 1.4 is still visible, although its energy level is low compared to that of the peak at St = 0.65. A further subharmonic at approximately St = 0.3 is also discernible. The -60dB energy contour for the upper shear layer lies almost on the jet centerline, r/D = 0, while the corresponding line for the lower shear layer is located at approximately r/D = -0.2.

A similar technique is demonstrated in Figures 26-28, which display the energy distribution in spatial coordinates r/D and $(x-x_0)/D$ for three radial

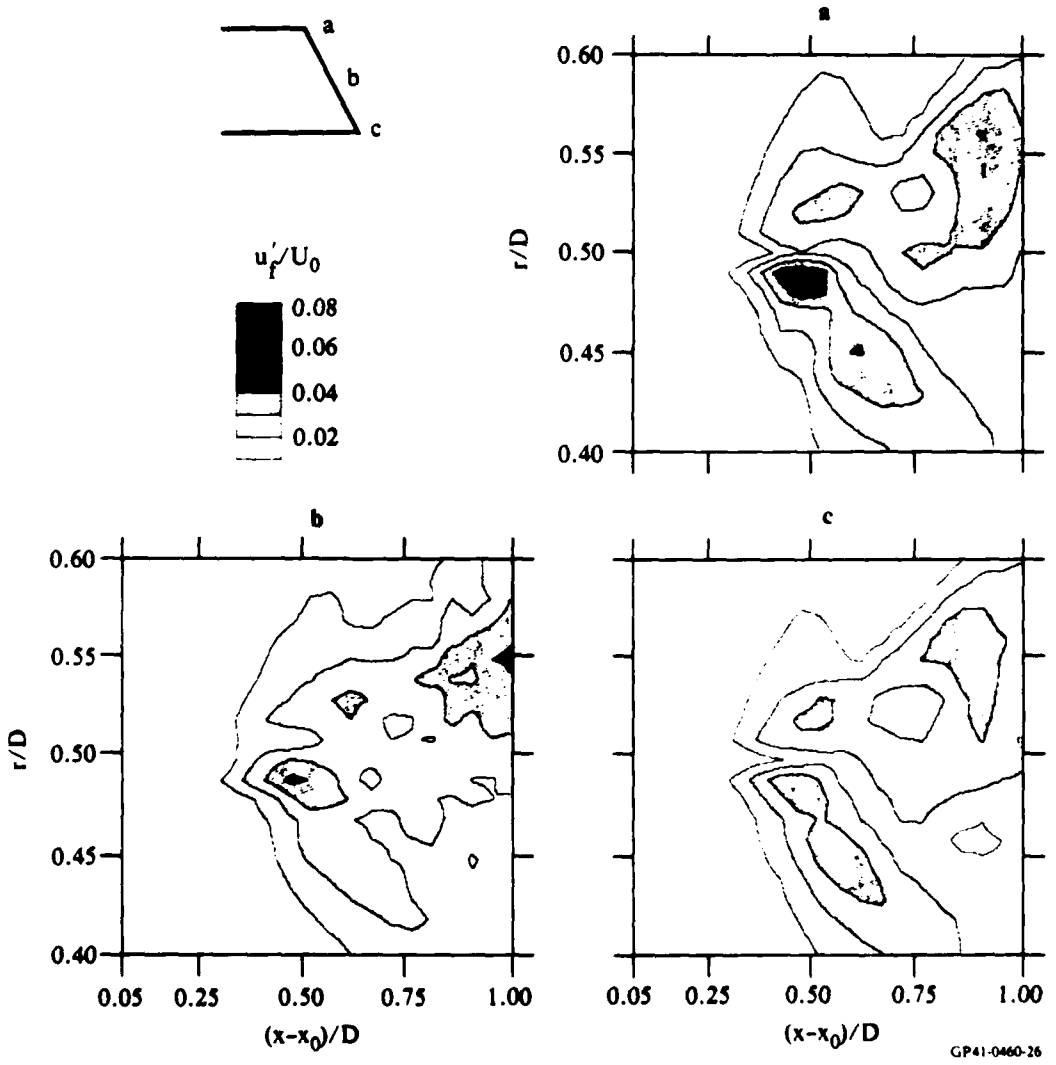

Figure 26. Azimuthal variation of f_s development; nozzle 1C; $U_0 = 30$ m/s.

planes corresponding to $\psi = 0^{o}$(c), 90^{o}(b), and 180^{o}(a). The scale of the radial coordinate is expanded by a factor of 2.5 compared to that for the streamwise coordinate. The maps display the equal-energy levels for hot-wire anemometer signals filtered at the primary shear-layer instability frequency f_s (Figure 26), at its subharmonic $f_s/2$ (Figure 27), and at the second subharmonic, $f_s/4$ (Figure 28). In Figure 26 all three maps exhibit a symmetry about the line r/D = 0.5. The beginning of the amplification of the waves corresponding to the shear layer frequency f_s begins at approximately the same distance from origin, $(x-x_o)/D$, for each azimuthal position, indicating that

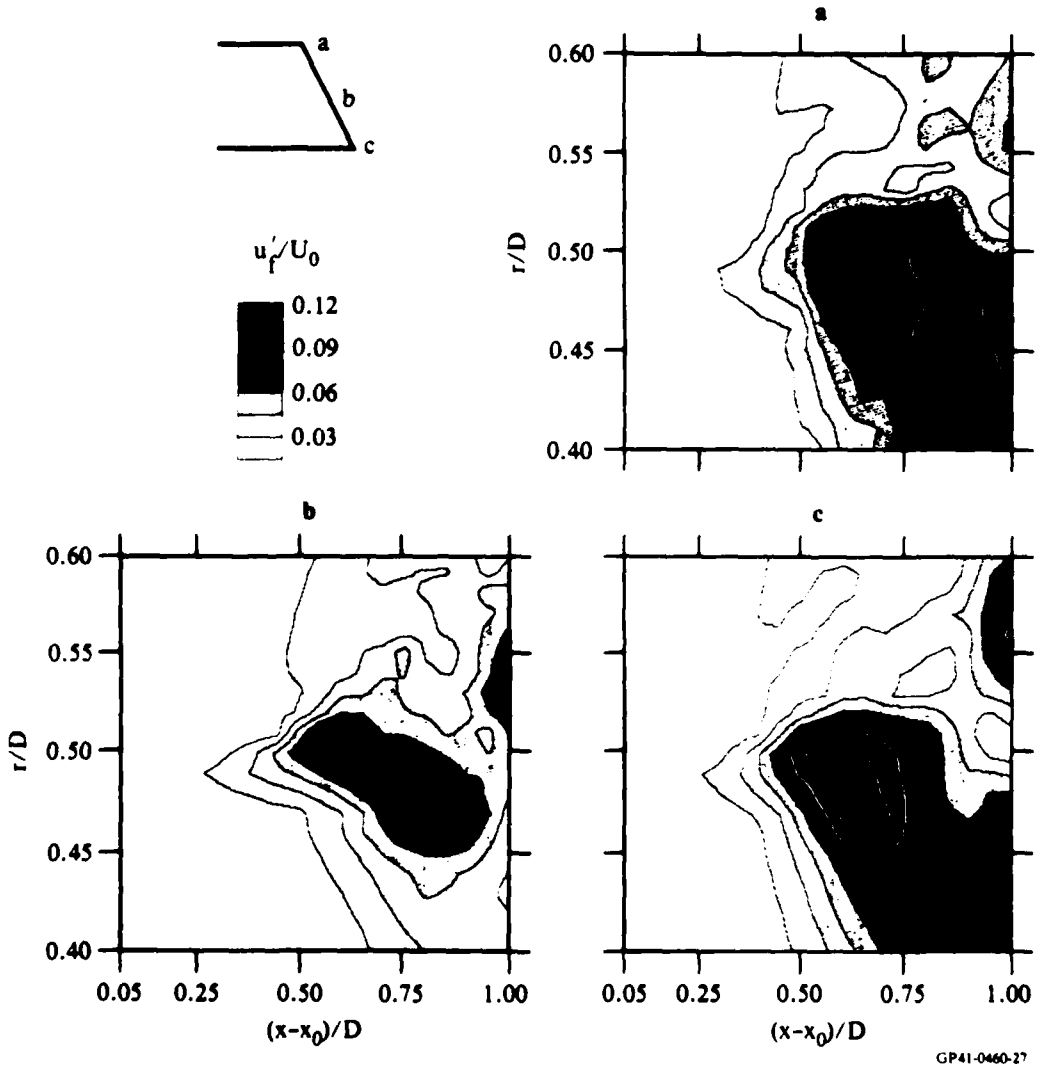

Figure 27. Azimuthal variation of $f_s/2$ development; nozzle 1C; $U_0 = 30$ m/s.

the system of instability waves represented here develops externally, with lines of constant phase aligned with the nozzle-exit inclination angle. Each map consists of a series of energy peaks at discrete locations above and below the centerline r/D = 0.5. In comparing these results with flow-visualization photographs, we can correlate energy maxima with locations at which nonlinearlity and vortex rollup are established. These events occur at effectively fixed streamwise locations and involve excursion of successive vortices into lateral orbits about each other, producing an organized vortex core having twice the wavelength of the previous system.

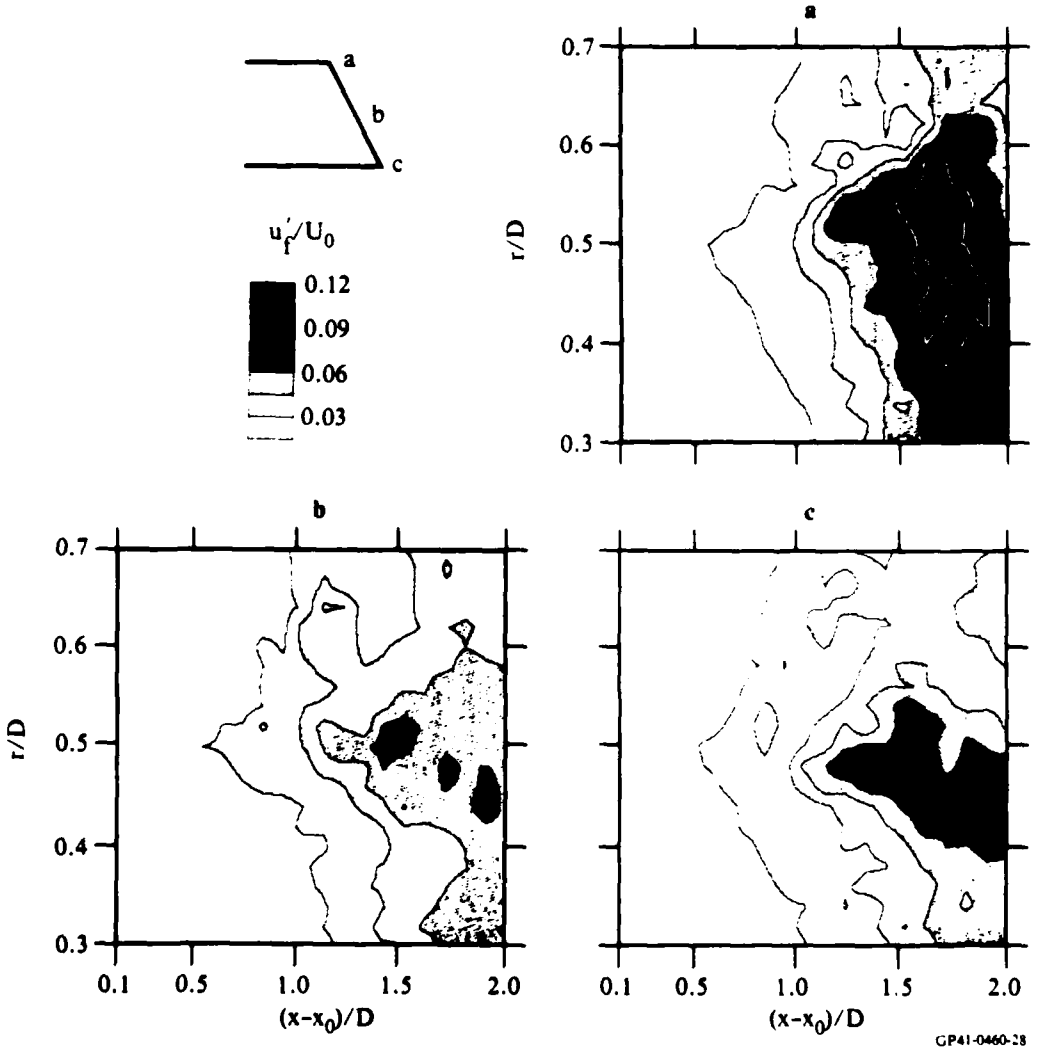

Figure 28. Azimuthal variation of $f_s/4$ development; nozzle 1C; $U_0 = 30$ m/s.

The maps of Figures 26a and 26c are qualitatively similar, although the energy peak in Figure 26a at $r/D = 0.48$ and $(x-x_o)/D = 0.5$ is stronger than the corresponding one in Figure 26c. These maps represent the periodically repeating process of vortex pairing whose recurring motion contributes energy at the same spatial locations. The map in Figure 26b, however, is distinct from the others, indicating that by the first pairing there is already a qualitative difference between the growth of the shear layers at the side locations compared to that of the upper and lower shear layers.

The discrepancy between the maps at the mutually orthogonal locations is considerably greater for the development of the subharmonic $f_s/2$ shown in Figure 27. Again, there is a similarity between Figures 27a and 27c for the upper and lower shear layers, while Figure 27b for the side shear layer is distinctly different. Whereas energy levels for the fundamental frequency were approximately the same for all three locations in Figure 26, the upper and lower shear layers are clearly more energetic than the side shear layers at the subharmonic frequency. Figure 27 suggests that over the range $0.5 \leq (x-x_o)/D \leq 1.0$, the upper and lower shear layers develop similar, strong vortex pairing activity, whereas the side shear layers generate much less pairing energy. When energy distributions for the second subharmonic are examined (Figure 28), the full three-dimensionality of the flow becomes evident in that all three azimuthal planes exhibit different patterns of turbulent activity, with the $\psi = 180^o$ plane being dominant.

4.5 Crenelated Nozzles and Secondary Effects

Although both slanted and stepped nozzles exhibit regions of high shear-layer momentum thickness growth, the overall conclusion regarding the crenelated nozzles is that they tend to suppress the formation of large turbulence scales and result in generally lower spreading rates than those of the reference nozzles. Crenelated-nozzle flowfields also exhibit some additional resonance-like effects.

Figure 29 shows the results of a test of a crenelated nozzle with two tabs. The data were taken from a microphone placed at the end of the tabs, one diameter from the nozzle centerline. Spectra were taken at the fixed microphone location as velocity of the flow was varied from 15 to 50 m/s. The flow was characterized by a series of audible tones whose center frequencies are plotted in the form of a Strouhal number vs. jet-exit velocity U_o. The

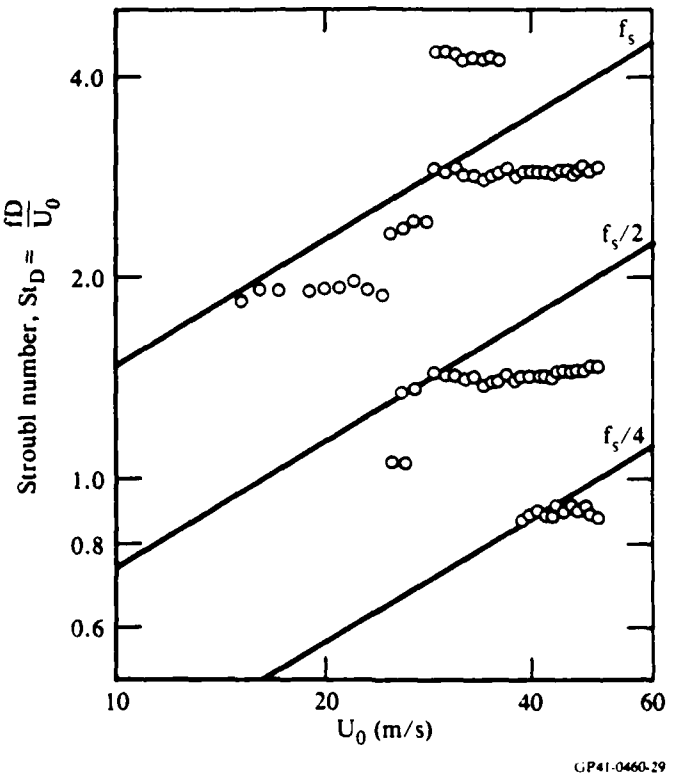

Figure 29. Near-field pressure spectrum peaks as a function of jet velocity for a two-tab crenelated nozzle; tab length = D/2; D = 25.4 mm.

distinctive feature of the plot is that frequency peaks appear to be locked to constant values of Strouhal number over wide velocity ranges. The solid lines represent observations made in the flowfield of a circular jet, with the upper line representing variation of the shear-layer instability frequency f_s with velocity, the next line $f_s/2$, etc. We offer no ready explanation for this phenomenon, although possible feedback from ends of the tabs is suggested. Similar, though less distinct, behavior is exhibited by a four-tab crenelated nozzle.

Pipe resonance can also enter as a secondary effect that modifies shear-layer properties of a given nozzle termination. The data for Figure 30 consist of spectral peaks from a microphone placed at the nominal end point of nozzle 1C, one diameter off axis. The data represent variation of peak frequencies as constant-diameter extension sections were inserted ahead of the termination. Velocity was adjusted for each length change to obtain a

resonance peak. The data indicate that the pipe-resonance frequency determines the shear-layer structure when resonance conditions exist and that it couples with the first subharmonic $f_s/2$ of the coherent structure development.

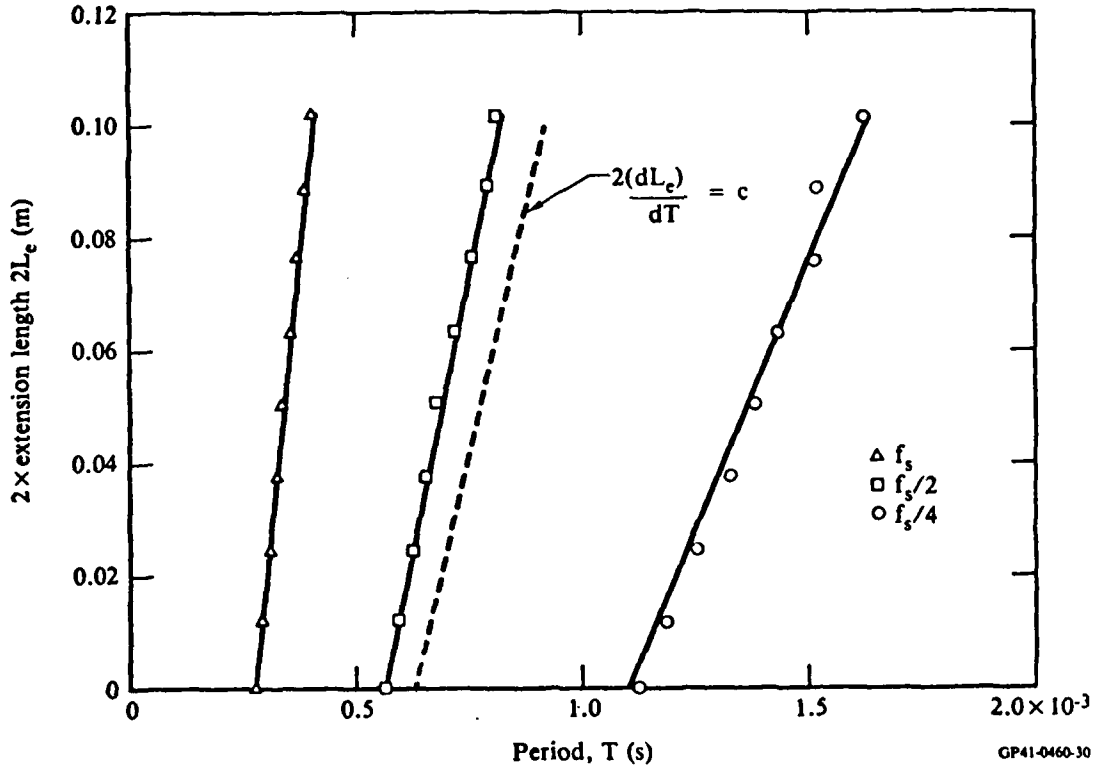

Figure 30. Variation of pipe resonance characteristics with pipe length for nozzle 1C.

5. PLANS FOR SECOND YEAR OF PROGRAM

In the second year of the program, we will investigate the active control concept as applied to inclined and stepped nozzle geometries selected from the first-year results.

The specific objectives will be:

1. Select and evaluate acoustical and mechanical excitation devices to be used with the nozzles selected above, including (a) a segmented acoustic exciter for the step-nozzle termination, (b) an acoustic exciter suitable for use with the slanted-nozzle termination, (c) a duct-integrated acoustic exciter for generating planar wave perturbations within the system, and (d) a mechanically driven oscillating exciter for generating discrete streamwise vorticity filaments.

2. Perform detailed flowfield tests including flow visualization and hot-wire surveys of mean and fluctuating flowfield properties, as in the first-year program.

3. Apply computer-based conditional sampling procedures to the excited flowfields using excitation signals to trigger phase-averaging algorithms.

4. Install an ejector shroud at the end of a constant-diameter-nozzle extension pipe forced by an acoustic, duct-integrated exciter and evaluate the active control effects of matching forced upstream duct resonance frequencies to the flowfield shear layer or jet-column instability and ejector shroud resonance frequencies.

5. Select nozzle and exciter combinations for experiments in feedback control.

In addition to mapping the extent of global influence that can be exerted using active control, we will also seek to clarify some fundamental questions that have emerged from the first-year program, such as: (1) What is the process whereby shear layer instabilities develop into internally or

externally generated wave systems? (2) What are the detailed steps whereby instability-wave systems acquire three-dimensionality and depart in character from axisymmetric flows with planar exits? (3) What is the phase relationship between the upper and lower shear layers? (4) What are the amplification rates of instability wave subharmonics? and (5) What is the azimuthal variation of subharmonic content along lines of constant phase?

Active control will be applied using externally powered acoustic exciters designed to inject uniform perturbation levels in the shear layers of I.O. nozzles. We have selected four stepped and slanted nozzles to generate flows for active control implementation. These are nozzle designations 1C, 2C, 1E, and 2E. We will use 63.5- and 24.5-mm external acoustic exciters for these nozzles, following the general exciter design used in previous MDRL excitation work. A schematic of exciters for stepped and slanted nozzles is shown in Figure 31. Each exciter consists of an external excitation chamber, sectioned in four parts surrounding the nozzles so each section has an equal settling volume ahead of the exciter exit slit. This design provides uniformity of excitation of all parts of the nozzle lip. Each sector of the chamber will have a separate driver tube, which connects to a common acoustic driver. Sectioning of the excitation chambers will make it possible to excite individual nozzle sectors independently to test the sensitivity of different parts of the nozzle lip to external perturbations.

An exciter will also be constructed for applying excitation within the flow system, as opposed to exciting the shear layer. It will consist of a segment of 63.5-mm pipe with four drivers positioned externally, communicating radially with the interior of the pipe through porous acoustic access ports having inner surfaces that are sufficiently smooth to result in minimal interference with the pipe boundary layer. The exciter will be positioned in the center of an extension tube that is attached to the nozzle contraction. Test nozzles will be attached to the end of the extension tube. Nozzle diameters used will be 63.5 mm, corresponding to the extension-tube diameter, and 24.5 mm, connecting to the extension tube through a secondary contraction. Excitation will be applied at a series of natural frequencies corresponding to standing wave patterns possible in the extension pipe. This method of excitation will provide intense plane-wave excitation that impinges uniformly on the exit and contains a surging flow component at the excitation frequency. A series of extension pipes of graduated length will be constructed to allow use of a sequence of pipe-resonance excitation frequencies.

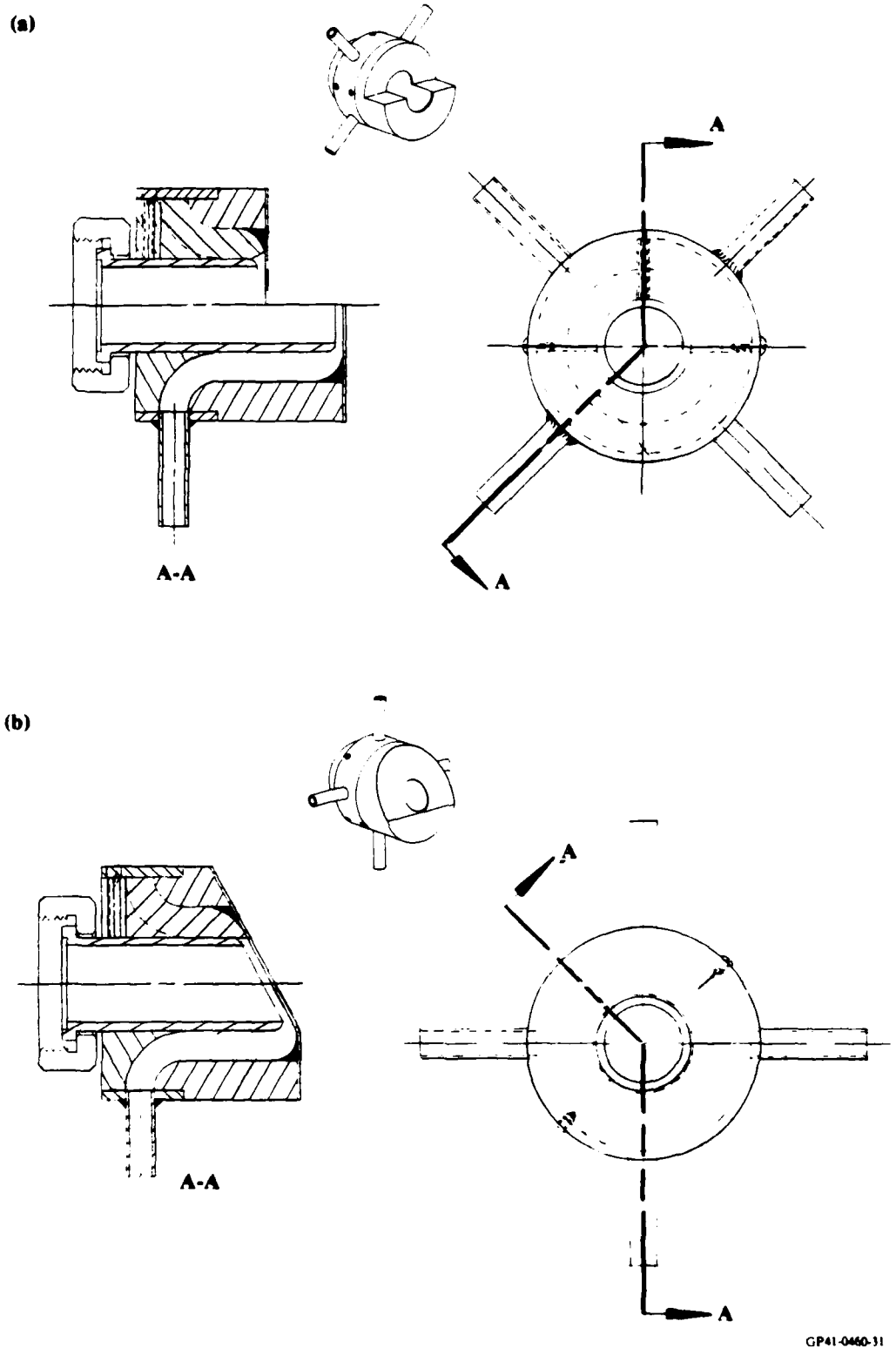

Figure 31. Acoustic excitation apparatus for (a) stepped and (b) slanted nozzles.

6. PUBLICATIONS

Results obtained during the first year of this program were described in the following presentations given at the American Physical Society meeting in Houston, Texas on 20-22 Nov, 1983, with abstracts published as follows:

V. Kibens and R. W. Wlezien, "Instability Waves in Jets with Indeterminate Origins," Bull. Am. Phys. Soc. 28, 9 (1983).

R. W. Wlezien and V. Kibens, "Modification of Jet Flowfields by Passive Control," Bull. Am. Phys. Soc. 28, 9 (1983).

A paper is being prepared for presentation at the 9th AIAA Aeroacoustics Conference to be held in Williamsburg, Virginia, 15-17 Oct. 1984:

R. W. Wlezien and V. Kibens, "Passive Control of Jets with Indeterminate Origins."

7. RELATED RESEARCH

The contract work is complemented by a related IRAD effort initiated in 1983, which consists of an experimental investigation of passive control achievable using the I.O. nozzles described above at supersonic flow rates up to a nozzle pressure ratio NPR = 4.0. Results of the IRAD tests indicate that wide variation in spreading rates and mean flow deflection angles, as well as highly asymmetric flow properties, are achievable. The supersonic work will be continued in the 1984 MDRL IRAD program and will consist of detailed investigations of the shock structures responsible for the observed effects. The 1984 MDRL program also includes acoustic testing of the I.O. nozzles at subsonic and supersonic nozzle pressure ratios. The tests will be conducted in cooperation with the Douglas Aircraft Company Acoustics Engineering Department at the DAC Anechoic Test Facility in El Segundo, California. The results of this work will be reported elsewhere.

8. REFERENCES

1. A. Krothapalli, D. Baganoff, and K. Karamcheti, "On the Mixing of a Rectangular Jet," J. Fluid Mech. 107, 201 (1981).

2. H. S. Husain and A.K.M.F. Hussain, "Controlled Excitation of Elliptic Jets", Phys. Fluids 26 (10), 2763 (1983).

3. V. Kibens, "The Limits of Initial Shear-Layer Influence on Jet Development," AIAA Paper 81-1960, 1981.

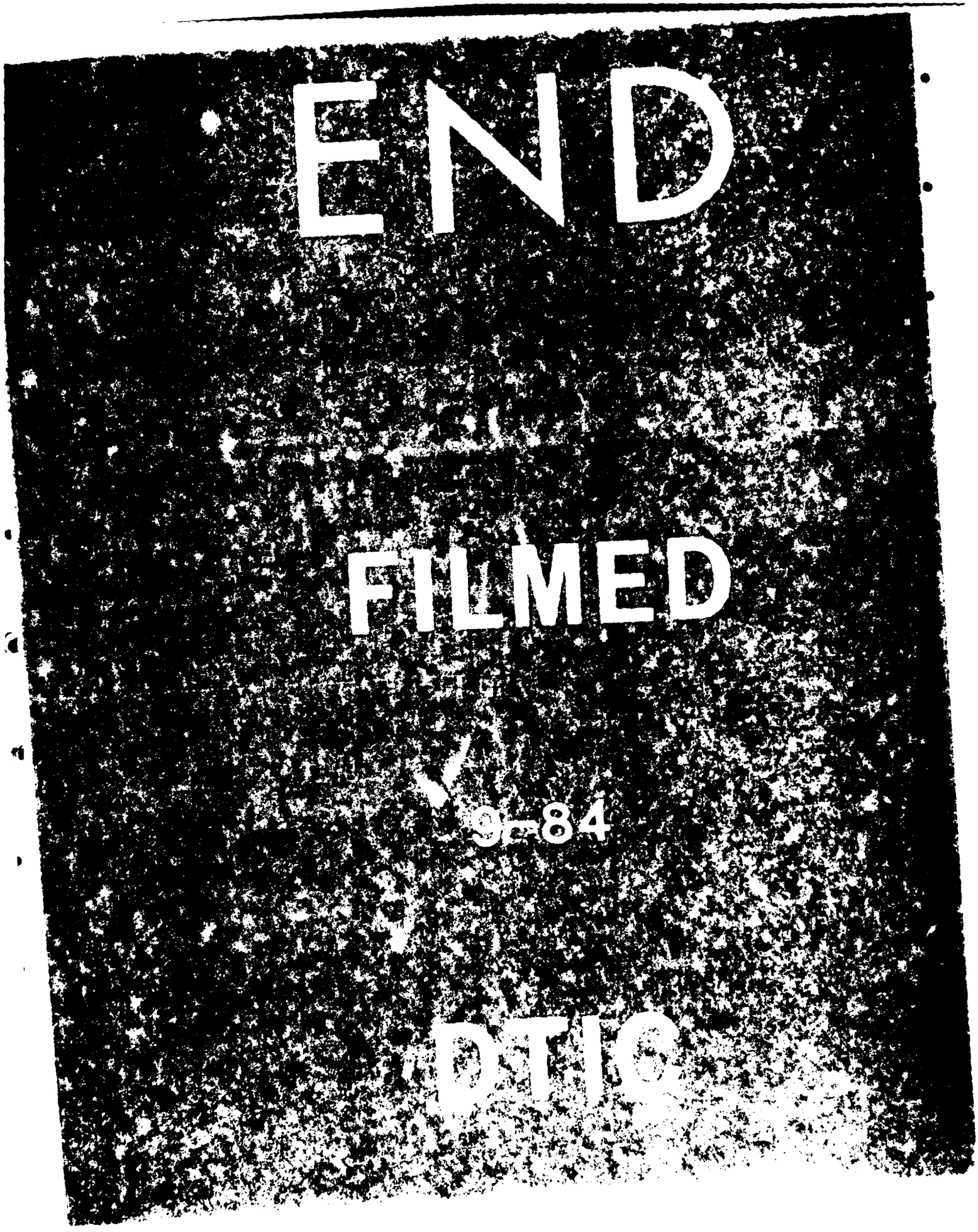
END
FILMED
9-84
DTIC